Available online at www.sciencedirect.com
SCIENCE DIRECT®
International Journal of Heat and Mass Transfer 47 (2004) 555–572
International Journal of HEAT and MASS TRANSFER
www.elsevier.com/locate/ijhmt

Monte Carlo modeling of radiative transfer in a turbulent sooty flame

Lionel Tessé [a,*], Francis Dupoirieux [a], Jean Taine [b]

[a] *Fundamental and Applied Energetics Department (DEFA), Office National d'Études et de Recherches Aérospatiales, Chemin de la Hunière, 91761 Palaiseau Cedex, France*

[b] *Laboratoire d'Énergétique Moléculaire et Macroscopique, Combustion (EM2C), UPR 288 du CNRS et de l'ECP, École Centrale Paris, 92295 Châtenay-Malabry Cedex, France*

Received 27 November 2002; received in revised form 15 June 2003

Abstract

The calculation of radiative transfer within a sooty turbulent ethylene–air diffusion jet flame has been carried out by using a Monte Carlo method and an accurate CK model for the gases. The influence of the turbulence–radiation interaction (TRI) has been studied. In the TRI modeling, the radiative properties of the assumed homogeneous turbulent structures are randomly obtained from a multidimensional probability density function (PDF) of the reaction progress variable, of the mixture ratio and of the soot volume fraction. This joint PDF is obtained from an Eulerian–Lagrangian turbulent combustion model and the sizes of the turbulent structures are directly derived from a k–ϵ model. In the considered flame, the TRI effect is an increase of the radiative heat loss by about 30%. The radiative heat loss becomes almost equal to one-third of the chemical heat release. Soot particles play the most important role in the global radiative heat loss but the influence of gaseous species like CO_2 and H_2O can be important in the local energy balance.

1. Introduction

In most of the flames, radiative transfer significantly influences the temperature field and hence the concentration of reactive species. On the other hand, the radiative power field strongly depends on the temperature and on the composition of the medium. There is a strong coupling between combustion and radiative transfer. In numerical simulations, this coupling can be treated by an iterative process. The purpose of this paper is to develop a radiative transfer approach, to be inserted in this iterative scheme, but not to iterate the procedure up to the convergence.

Different techniques, i.e. a method of resolution of the radiative transfer equation associated with a model for the radiative properties, have been used to calculate the radiative power per unit volume, in the energy balance of a sooty flame. In many cases, e.g. [1–7], these flames are laminar or, if they are turbulent, the effects of the turbulent fluctuations on the radiative transfer have been neglected. De Lataillade [1] has calculated a 1D countercurrent laminar diffusion flame of methane by using a radiative Monte Carlo method based on the reciprocity principle. Soot particles have been taken into account and radiative properties of gases, i.e. H_2O, CO_2 and CO, have been modeled with a statistical narrow band model formulated in k-distribution. Zhang and Ezekoye [2] have used a discrete ordinates method (DOM) for a methane–air diffusion flame considered as a gray medium. Bressloff et al. [3] have calculated a turbulent methane–air diffusion flame by using a discrete transfer method associated with a weighted sum of gray gas model. Kaplan et al. [4] have used a DOM for unsteady laminar ethylene diffusion flames assumed to be gray media. Sivathanu and Gore [5] have used a ray-tracing method to point out the strong coupling between soot formation and radiation in laminar acetylene diffusion flames, supposed to be only composed of gray soot particles. For a laminar ethylene diffusion flame, Kent and Honnery [6] have only considered the

* Corresponding author.
E-mail address: lionel.tesse@onera.fr (L. Tessé).

0017-9310/$ - see front matter © 2003 Elsevier Ltd. All rights reserved.
doi:10.1016/j.ijheatmasstransfer.2003.06.003

Nomenclature

B	source point of an optical path
c_i, c_q	chemical concentration of the cell i, of the cell q
c_{i_q}	sequence of the chemical concentrations along an optical path linking the cells i and q
c_s	chemical concentration in the turbulent structure of index s
C_μ	constant of the turbulence model (equal to 0.09)
f	probability density function (PDF)
f_V	soot volume fraction
F	inlet point of an optical path in a volume cell
i	cell index
j	index of crossing of a given cell by an optical path along this optical path
$I_v^0(T)$	equilibrium (or blackbody) spectral intensity ($W\,m^{-2}\,(cm^{-1})^{-1}\,sr^{-1}$)
k	turbulent kinetic energy ($m^2\,s^{-2}$)
l_{ts}	integral length scale of the turbulent structure of index s (m)
M	inlet point of an optical path in a coherent turbulent structure
n	index of the turbulent structure surrounding the point F of the absorbing cell
N_i	number of optical paths issued from the cell i
N_{iq}	number of optical paths originating from the cell i and crossing or encountering the cell q
N_c	total number of crossings of a given cell by an optical path
N_r	number of wall reflections along an optical path
N_S	number of cells made of a piece of surface (wall or boundary)
N_V	number of volume cells
p	optical path index
P_i^e	total power emitted by the cell i (W)
P_{iq}^{ea}	power emitted by the cell i and absorbed by the cell q (W)
P_{iq}^{exch}	power exchanged between the cells i and q (W)
P_i^{FM}	radiative power in the cell i given by the forward method (W)
P_i^{REC}	radiative power in the cell i given by reciprocal methods (W)
q	cell index
r	mixture ratio (r is equal to 1 at stoichiometry)
s	turbulent structure index along an optical path
T_i, T_q	temperature of the cell i, of the cell q (K)
T_{i_q}	sequence of the temperatures along an optical path linking the cells i and q (K)
T_s	temperature in the turbulent structure of index s (K)

Greek symbols

α_{qv}	spectral absorptivity in the cell q
Δ	initial direction of the optical path
ϵ	dissipation rate of the turbulent kinetic energy ($m^2\,s^{-3}$)
ε_{wiv}	spectral emissivity of the wall i
κ_{iv}	spectral absorption coefficient of the cell i (m^{-1})
v	wavenumber (cm^{-1})
θ	polar angle
$\tau_v(BF)$	spectral transmissivity between the points B and F
Ω	solid angle (sr)
ξ	progress variable of the chemical reactions
Ψ_i, Ψ_q	PDF of T and c in the cell i, in the cell q
Ψ_s	PDF of T and c in the turbulent structure of index s

Notations

$\widetilde{(\ )}$	Monte Carlo statistical estimation (average over the contributions of the optical paths)
$\langle\ \rangle$	statistical (temporal) mean of a turbulent quantity
$\|MF\|$	distance between the points M and F (m)

contribution of the soot particles, assumed to be gray, by using a DOM. Said et al. [7] have developed a new Eulerian–Lagrangian model of soot production in turbulent flames, associated with the optically thin limit (OTL) assumption.

In turbulent flames, the influence of the fluctuations on the radiative transfer has to be considered. For instance, in the flamelet regime, when the mean temperature is 1300 K, the temperature probability density function (PDF) can be made of two peaks, at 600 and 2000 K, respectively; the fluctuations are then of the same order of magnitude as the averaged values and generate strong non-linear effects on both emitted intensities and radiative properties. Faeth and coworkers [8–12] have studied experimentally and numerically turbulent diffusion flames of methane, ethylene, carbon monoxide, acetylene and hydrogen. They have calculated intensities along a ray by taking into account the

turbulence–radiation interaction (TRI) and have concluded that its effect on the radiative transfer is very important (50–300%), especially in ethylene, acetylene and hydrogen flames. Their TRI modeling is based on the partitioning of an optical path into a set of independent coherent turbulent structures, supposed to be homogeneous and isothermal. The size of a structure is proportional to the associated turbulence integral length scale. The thermophysical properties of a structure, i.e. the temperature, the soot volume fraction and the molar fraction of the gaseous species, are randomly obtained from a 1D PDF of the mixture fraction. The radiative properties are given by the RADCAL code. Syed et al. [13] have applied the same approach to a methane flame after improvement of the evaluation of the soot volume fraction. Mazumder and Modest [14] have calculated the radiative transfer in a methane diffusion flame with a spherical harmonics method (SHM), associated with the optically thin fluctuation assumption (OTFA) [15,16], to partially take into account the TRI. Soot particles are not considered and radiative properties of gases, i.e. H_2O, CO_2 and CH_4, are calculated with a box model involving 10 wide bands. They have used a stochastic Lagrangian method to evaluate the correlation between the temperature and mass fraction fluctuations. The TRI leads to an increase by 40–45% of the radiative wall fluxes. Adams and Smith [17] have used a DOM associated with the OTFA in an industrial furnace, assumed to be a gray medium. The fluctuations of the thermophysical properties have been deduced from a 2D PDF of the mixture ratio and of the total enthalpy. Hartick et al. [18] have used a similar approach. Young and Moss [19] have developed a method based on a tabulation of the radiative heat loss as a function of the thermophysical properties.

To calculate radiative transfer by taking into account the turbulence–radiation interaction, the usual deterministic methods (DOM, SHM...) require, in practice, some simplifying assumptions, i.e. OTFA and assumptions on gas radiative properties. On the other hand, a stochastic Monte Carlo method, which does not require these assumptions, is convenient for radiative transfer calculations in turbulent flames.

The Monte Carlo approaches in use here have been developed and validated for averaged temperature and concentration fields in a previous work [20]. It is now generalized to the calculation of TRI effects in turbulent sooty flames, considered as emitting, absorbing but non-scattering media, typical of reactive flows in some industrial combustors from the points of view of radiation emission and turbulence intensity. To model the TRI, the method developed by Faeth and coworkers [8–12] along a single ray has been improved and extended to the calculation of the radiative power in the whole flame. The thermophysical properties of a turbulent structure are randomly obtained from a 3D PDF of the reaction progress variable, of the mixture ratio and of the soot volume fraction. This joint PDF is obtained from an Eulerian–Lagrangian turbulent combustion model [21] and the sizes of the turbulent structures are directly derived from a k–ϵ model. Gas radiative properties are calculated with a CK model [22] involving more than 1000 pseudo-spectral points.

The Monte Carlo modeling of the TRI is detailed in Section 2. A turbulent ethylene–air jet sooty flame, its combustion modeling and the radiative properties models are described in Section 3. Results obtained for this flame are presented in Section 4. The influence of the TRI and of the soot particles are discussed.

2. Monte Carlo modeling of the turbulence–radiation interaction

2.1. General formulation

In a Monte Carlo method, the unknown quantities to be calculated are weighted by the joint PDF of the physical parameters that characterize the system. These unknown quantities are here the radiative power or flux in each cell of the calculation grid. They can be calculated by different methods based either on the reciprocity principle or on the usual forward formulation of the Monte Carlo method [20,23]. In the reciprocal approaches, the radiative power P_q^{REC} in the cell q is given by

$$P_q^{\mathrm{REC}} = -\sum_{i=1}^{N_{\mathrm{V}}+N_{\mathrm{S}}} P_{iq}^{\mathrm{exch}}, \tag{1}$$

where P_{iq}^{exch} is the radiative power exchanged between the cells i and q. In the forward formulation, the radiative power P_q^{FM} is obtained by

$$P_q^{\mathrm{FM}} = \left(\sum_{i=1}^{N_{\mathrm{V}}+N_{\mathrm{S}}} P_{iq}^{\mathrm{ea}}\right) - P_q^{\mathrm{e}}, \tag{2}$$

where P_{iq}^{ea} is the radiative power emitted by the cell i and absorbed by the cell q and P_q^{e} the total power emitted by the cell q. Without turbulence effects, P_{iq}^{exch} is given by Eq. (8) of Ref. [20], i.e.

$$P_{iq}^{\mathrm{exch}} = P_i^{\mathrm{e}} \int_0^{+\infty} \left(\frac{I_\nu^0(T_q)}{I_\nu^0(T_i)} - 1\right) \int_{V_i} \int_{4\pi} \sum_{j=1}^{N_{\mathrm{c}}} \tau_\nu(BF_j)\alpha_{q_j\nu} \times f_i(B,\Delta,\nu)\,\mathrm{d}\Omega_i\,\mathrm{d}V_i\,\mathrm{d}\nu, \tag{3}$$

where the PDF $f_i(B,\Delta,\nu)$ is given by

$$f_i(B,\Delta,\nu) = \frac{\kappa_{i\nu} I_\nu^0(T_i)}{P_i^{\mathrm{e}}}, \tag{4}$$

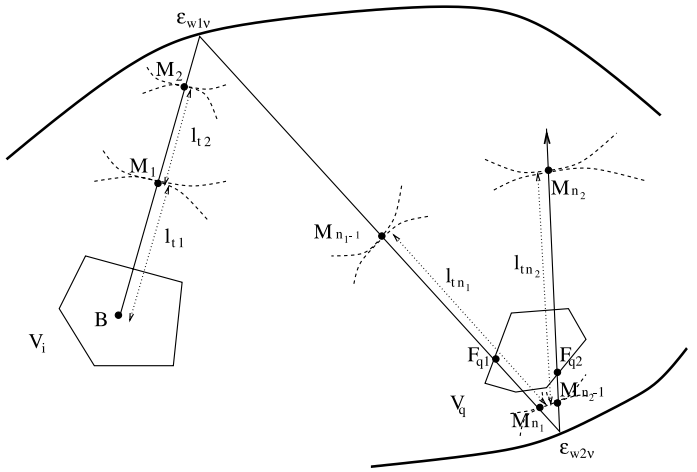

Fig. 1. Principle of the radiative power transmission from cell i to cell q.

if the cell i is a volume, or by

$$f_i(B,\Delta,\nu)=\frac{\varepsilon_{wi\nu}I^0_\nu(T_i)\cos\theta_i}{P^e_i}, \tag{5}$$

if the cell i is a surface (the integration over dV_i is replaced by an integration over dS_i). B and F_j are the points of the cells i and q defined in Fig. 1. $\tau_\nu(BF_j)$ is the spectral transmissivity between the points B and F_j, including possible reflections on walls or on boundaries. The sum on the index j accounts for the N_c crossings through the cell q along the same optical path. $\alpha_{q_j\nu}$ is the absorptivity of the cell q associated with the jth crossing. $\varepsilon_{wi\nu}$ is the emissivity of the cell i if this cell is a wall element and θ_i is the angle between the optical path and the direction normal to the wall. P^{ea}_{iq} is given by an equation similar to Eq. (3), i.e.

$$P^{ea}_{iq}=P^e_i\int_0^{+\infty}\int_{V_i}\int_{4\pi}\sum_{j=1}^{N_c}\tau_\nu(BF_j)\alpha_{q_j\nu}f_i(B,\Delta,\nu)\,d\Omega_i\,dV_i\,d\nu. \tag{6}$$

As the method in use to calculate P^{ea}_{iq} can also be applied to the calculation of P^{exch}_{iq}, only the formulation dealing with P^{ea}_{iq} will be here developed.

If we also consider turbulent fluctuations, $I^0_\nu(T_i)$, $I^0_\nu(T_q)$, $\tau_\nu(BF_j)$, $\alpha_{q_j\nu}$ and $\kappa_{i\nu}$ must be stochastically modeled because these quantities depend on the instantaneous local temperature and composition fields in the medium. Let us introduce the joint PDF Ψ of the temperature T and of the chemical concentrations c defined in all the cells of the flow (c is a vector of which the components are the concentrations of the chemical species involved in the radiative transfer, i.e. H_2O, CO_2 and soots). Eq. (6) becomes in the case of a turbulent flow

$$\langle P^{ea}_{iq}\rangle=\int_{T,c}P^e_i\left[\int_0^{+\infty}\int_{V_i}\int_{4\pi}\sum_{j=1}^{N_c}\tau_\nu(BF_j)\alpha_{q_j\nu}f_i(B,\Delta,\nu)\,d\Omega_i\,dV_i\,d\nu\right]\times\Psi(T_{i\_q},c_{i\_q})\,dT_{i\_q}\,dc_{i\_q}. \tag{7}$$

In this equation, the quantities P^e_i, τ_ν, $\alpha_{q_j\nu}$ and f_i are defined at a given time and the radiation propagation is assumed instantaneous. The power $\langle P^{ea}_{iq}\rangle$ is averaged by using the joint PDF Ψ in which T_{i_q} stands for all the temperatures involved in the quantities P^e_i, τ_ν, $\alpha_{q_j\nu}$ and f_i and c_{i_q} for all the chemical concentrations involved in the same quantities. These temperatures and concentrations must be defined not only in cells i and q but also along all the optical paths BF_j.

If we take into account the turbulence effects, the mean radiative power in the cell q, in the forward formulation, is given by

$$\langle P^{FM}_q\rangle=\left(\sum_{i=1}^{N_V+N_S}\langle P^{ea}_{iq}\rangle\right)-\langle P^e_q\rangle, \tag{8}$$

where the mean total power $\langle P^e_q\rangle$ emitted by the cell q is defined by

$$\langle P^e_q\rangle=4\pi V_q\int_{T_q,c_q}\int_0^\infty\kappa_\nu(T_q,c_q)I^0_\nu(T_q)\Psi_q(T_q,c_q)\,d\nu\,dT_q\,dc_q. \tag{9}$$

2.2. Modeling of turbulence structures

The turbulence field is spatially correlated, i.e. the physical properties of the medium are strongly correlated along an element of optical path included in a given coherent structure, but are not correlated with the physical properties of the following structure. A typical scale of the coherent turbulent structure is the turbulent integral length l_t, deduced in each mesh of the calculation grid from the values of the turbulent kinetic energy k and of its dissipation rate ϵ issued from the fluid mechanics calculations, i.e.

$$l_t=C_\mu^{3/4}\frac{k^{3/2}}{\epsilon}. \tag{10}$$

We consider here a simple formulation in which all the properties of the medium are assumed uniform along the integral length l_{ts} of each coherent structure s successively crossed by an optical path. When an optical path is generated in point B located in structure $s = 1$ (see Fig. 1), the temperature and concentrations T_1 and c_1 are randomly determined from the PDF Ψ_1 associated with the first coherent turbulent structure of length l_{t1}, from B to M_1, whatever the number of cells crossed inside the structure. At the point M_1, new temperature and concentrations are randomly determined by using the joint PDF Ψ_2 defined in the cell containing M_1 and a new integral length scale l_{t2} is also calculated. The process is iterated until the transmitted fraction of the power emitted from B is less than a given cutoff criterion. In the case of the diffusion flame considered in the following, 3–4 cells are typically crossed before new temperature and concentrations are randomly determined. A more sophisticated turbulence model could be easily implemented in the same Monte Carlo method, but we focus here on radiative transfer calculations, not on turbulence modeling. However, the influence of the value of l_t is discussed in Section 4.2.

According to the chosen turbulence model, the joint PDF Ψ can be rewritten as

$$\Psi(T_{i\_q}, c_{i\_q})\mathrm{d}T_{i\_q}\,\mathrm{d}c_{i\_q} = \prod_{s=1}^{n_j+a} \Psi_s(T_s, c_s)\,\mathrm{d}T_s\,\mathrm{d}c_s, \tag{11}$$

where n_j is the total number of turbulent structures crossed by the optical path between the point B and the point F_j belonging to the n_jth structure. Ψ_s is the joint PDF of the temperature T_s and of the concentrations c_s in the s th turbulent structure. The indices associated with T and c now correspond to a turbulent structure and not to a cell. If the cell q is included in the n_jth structure, a is equal to zero. On the contrary, if the n_jth structure ends into the cell q, a is equal to 1 and the index s has to vary from 1 to $n_j + 1$ in Eq. (11).

2.3. Stochastic Monte Carlo formulation

The principle of the Monte Carlo approach is to replace the multiple integral of Eq. (7) by a finite sum on a large number of optical paths. These optical paths are stochastically generated from the cell i by using the PDF's f_i and Ψ_s. With the same steps as those leading to Eq. (10) of paper [20], the following statistical estimation of $\langle P_{iq}^{ea} \rangle$ can be derived

$$\widetilde{\langle P_{iq}^{ea} \rangle} = \frac{1}{N_i} \sum_{p=1}^{N_{iq}} P_{i_p}^{e} \sum_{j=1}^{N_{cp}} \tau_{v_p}(B_{i_p}, F_{q_{pj}}) \sum_{s=n_{pj}}^{n_{pj}+1} \tau_{q_s v_p} \alpha_{q_s v_p}, \tag{12}$$

where N_i is the total number of optical paths issued from the cell i and N_{iq} the number of optical paths issued from the cell i and crossing the cell q. The spectral transmissivity between the points B_{i_p} and $F_{q_{pj}}$ is expressed as

$$\tau_{v_p}(B_{i_p}, F_{q_{pj}}) = \exp\left[-\sum_{s=1}^{n_{pj}-1} \kappa_{v_p}(T_s, c_s) l_{ts} \right] \exp[-\kappa_{v_p}(T_{n_{pj}}, c_{n_{pj}}) \times \|M_{n_{pj}-1} F_{q_{pj}}\|] \prod_{h=1}^{N_{rpj}} (1 - \varepsilon_{w_h v_p}), \tag{13}$$

where the couples (T_s, c_s) and $(T_{n_{pj}}, c_{n_{pj}})$ are randomly generated along the pth optical path using respectively the PDF's Ψ_s and $\Psi_{n_{pj}}$. N_{rpj} is the number of wall reflections along the pth optical path between the points B_{i_p} and $F_{q_{pj}}$, h the corresponding index and $\varepsilon_{w_h v_p}$ the local wall spectral emissivity. $\tau_{v_p}(B_{i_p}, F_{q_{pj}})$ is calculated by using the radiative models of Section 3.4.

In Eq. (12), the sum on the index s is introduced to treat the possibility that the end of the n_{pj}th turbulent structure is inside the cell q. If the whole cell q is included in the n_{pj}th turbulent structure, the product $\tau_{q_s v_p} \alpha_{q_s v_p}$ is defined by

$$\text{for } s = n_{pj}, \quad \tau_{q_s v_p} \alpha_{q_s v_p} = \alpha_{q_s v_p} = 1 - \exp[-\kappa_{v_p}(T_s, c_s) l_{q_{pj}}], \tag{14a}$$

$$\text{for } s = n_{pj} + 1, \quad \tau_{q_s v_p} \alpha_{q_s v_p} = 0, \tag{14b}$$

where $l_{q_{pj}}$ is the crossing distance through the cell q of the pth optical path for the jth crossing. If, on the contrary, the optical path crosses the outlet border of the n_{pj}th turbulent structure in the cell q, τ_{qsv_p} and α_{qsv_p} are given by

$$\text{for } s = n_{pj}, \quad \tau_{q_s v_p} \alpha_{q_s v_p} = \alpha_{q_s v_p} = 1 - \exp[-\kappa_{v_p}(T_s, c_s) \|F_{q_{pj}} M_s\|], \tag{15a}$$

$$\text{for } s = n_{pj} + 1, \quad \tau_{q_s v_p} = 1 - \alpha_{q n_{pj} v_p}, \tag{15b}$$

$$\alpha_{q_s v_p} = 1 - \exp\left[-\kappa_{v_p}(T_s, c_s)[l_{q_{pj}} - \|F_{q_{pj}} M_{n_{pj}}\|] \right]. \tag{15c}$$

The transposition of Eq. (12) to the case of a surface cell is straightforward.

When the cell i is a volume, the quantity $P_{i_p}^{e}$ depends on the stochastic values of the temperature $T_{i_{p1}}$ and of the concentrations $c_{i_{p1}}$ characterizing the first turbulent structure ($s = 1$) crossed by the pth optical path issued from the cell i. Consequently, it must be calculated for each optical path by

$$P_{i_p}^{e} = 4\pi V_i \int_0^{\infty} \kappa_v(T_{i_{p1}}, c_{i_{p1}}) I_v^0(T_{i_{p1}})\,\mathrm{d}v. \tag{16}$$

For a surface cell i, P_i^{e} does not depend on the optical path and is calculated only once.

The numerical procedure is the same as in Ref. [20], except two points. First, many additional stochastic number generations according to the PDF's Ψ_s are necessary to obtain the temperature and concentration fields on which the medium radiative properties depend. Moreover, the source point B_{i_p}, the initial direction Δ of the optical path and the wavenumber v_p are stochastically generated by using the PDF f_{i_p} which is now

$$f_{i_p} = \frac{\kappa_\nu(T_{i_{p1}}, c_{i_{p1}}) I^0_\nu(T_{i_{p1}})}{P^{\mathrm{e}}_{i_p}}, \tag{17}$$

where $P^{\mathrm{e}}_{i_p}$ is defined by Eq. (16).

The statistical estimation $\langle \widetilde{P^{\mathrm{exch}}_{iq}} \rangle$ of $\langle P^{\mathrm{exch}}_{iq} \rangle$ can be obtained in a very similar way, i.e. by Eq. (12) in which the term $(I^0_{\nu_p}(T_{q_s})/I^0_{\nu_p}(T_{i_{p1}}) - 1)$ is introduced. The radiative power is then deduced from $\langle \widetilde{P^{\mathrm{exch}}_{iq}} \rangle$ by using Eq. (1) in the case of a reciprocal method or from $\langle \widetilde{P^{\mathrm{ea}}_{iq}} \rangle$ by using Eq. (2) in the case of the forward method.

Let us note that the effects of the correlations between emission and absorption properties are rigorously taken into account. If the cells i and q are included in the first turbulent structure, the transmissivities $\tau_{\nu_p}(B_{i_p}, F_{q_{p1}})$ and $\tau_{q_1\nu_p}$ and the absorptivity $\alpha_{q_1\nu_p}$ are calculated with the same thermophysical properties as for the calculation of the emission parameters $\kappa_{\nu_p}(T_{i_{p1}}, c_{i_{p1}})$ and $I^0_{\nu_p}(T_{i_{p1}})$. Moreover, no additional assumption, like the OTFA, is required in this numerical treatment.

3. Application to a turbulent sooty ethylene–air flame

3.1. Experimental reference flame

We consider here an open diffusion flame which has been experimentally studied at the university of Rouen [24]. This flame has been chosen because its geometry is simple, the turbulence intensity in the reactive zone is high and some measurements of temperature and soot volume fraction are available. Pure gaseous ethylene is injected vertically upward in atmospheric air. Different injection velocity conditions have been experimentally used but we only consider here the largest velocity, 29.5 m/s, which leads to a significantly high turbulence level. The injection duct diameter is 4 mm, so that the global Reynolds and Froude numbers near the inlet are respectively 12000 and 22200. The flame holds at the confluence of injected ethylene and air, just at the outlet of the injection pipe and expands rapidly downstream because of the turbulent mixing. First, the measured temperature increases rapidly along the axis, then more slowly until 1600 K, value reached at 40 cm from the inlet. The temperature then gently decreases due to the air dilution. The evolution of the measured soot volume fraction is similar. However, the soot volume fraction increase is slightly shifted downstream, compared to the temperature increase, because of finite rate chemistry effects. The soot volume fraction decrease is much sharper than the temperature one because of the soot oxidation in addition to the air dilution. The maximum soot volume fraction, which is about 2 ppm, is obtained at 40 cm from the ethylene injection. The paper [21] displays very satisfactory comparisons about the temperature and the soot volume fraction between these measurements and the combustion calculation supplying all the information required by the present radiative transfer model.

3.2. Combustion modeling

The calculation of the radiative power requires the knowledge of the averaged fields of temperature and radiating species concentrations. Moreover, to account for the turbulence effects, the joint PDF field of all these quantities must be known. In this section, we remind the main steps of the procedure used to obtain this information. The details of the calculation are given in Ref. [21].

In the following, due to the symmetry about the flame axis, the computational domain, used both for combustion data and radiative calculations, reduces to a sector of 5° of a cylinder, i.e. 1/72 of the whole physical domain. The cylinder height and radius are respectively equal to 1 and 0.25 m. The discretization grid is structured but non-uniform and includes 150 cells in the axial direction, 60 cells in the radial direction and 1 cell in the orthoradial direction.

In a first step, a Reynolds averaged Navier–Stokes (RANS) calculation using a k–ϵ model adapted to jet flows gives some of the required average fields. In order to correct the temperature field, a source term crudely simulating the radiative loss has been introduced in the energy balance, i.e.

$$P^R = -\rho\dot{\omega}_F h^* \int_0^{+\infty} \exp\left[-\left(\frac{\ln r}{2\sigma}\right)^2\right] f(r)\,\mathrm{d}r. \tag{18}$$

ρ is the medium density, $\dot{\omega}_F$ is the reaction rate, $f(r)$ is a β-shaped PDF of the mixture ratio r (equal to 1 at stoichiometry) and h^* and σ are adjusted parameters introduced in order to match the axial measurements. This calculation is achieved with a simple combustion model (fast chemistry) and does not give any information on minor species, especially the soot particles.

In a second step, a Lagrangian calculation of the flow is carried out. A large number of fluid packets are tracked in the flow. The trajectory and the thermochemical evolution of these packets are computed by resolution of time dependent differential equations which take into account the complete chemical process: the chemistry in the gas is described by 38 species and 119 reactions while five parameters are used to describe the soot particle behavior (the concentration of two types of soot precursors, light and heavy, the number of particles per unit volume, the average particle size and the volume fraction). Let us note that the three last parameters are independent since the particle sizes are distributed on a large size range. The hydrocarbon species until C_6H_6 appear directly in the chemical kinetics, whereas heavier species are considered as a part of the light or heavy soot precursors, which are treated

in a global way. Concerning the soot particles, the phenomena of nucleation, surface growth, coalescence and oxidation are taken into account through source terms in the Lagrangian evolution equations. At a given time, the fluid packets give a local instantaneous picture of the flow. Therefore it is possible to deduce, in each cell of the grid used for the RANS calculation, the joint PDF of all the required quantities by reckoning all the fluid packets going through the cell and considering the value of the different parameters (temperature, concentrations, soot volume fraction) inside the cell. In the same way, all the mean quantities can be obtained in each cell by averaging on all the packets going through.

For ethylene–air sooty flames, the soot volume fraction which strongly influences the radiative transfer has to be accurately calculated. For that reason, it has been checked that the soot volume fraction given by the Lagrangian calculation is in agreement with the measurements made along the axis of the flame. Figs. 2 and 3 display the average temperature field, the soot

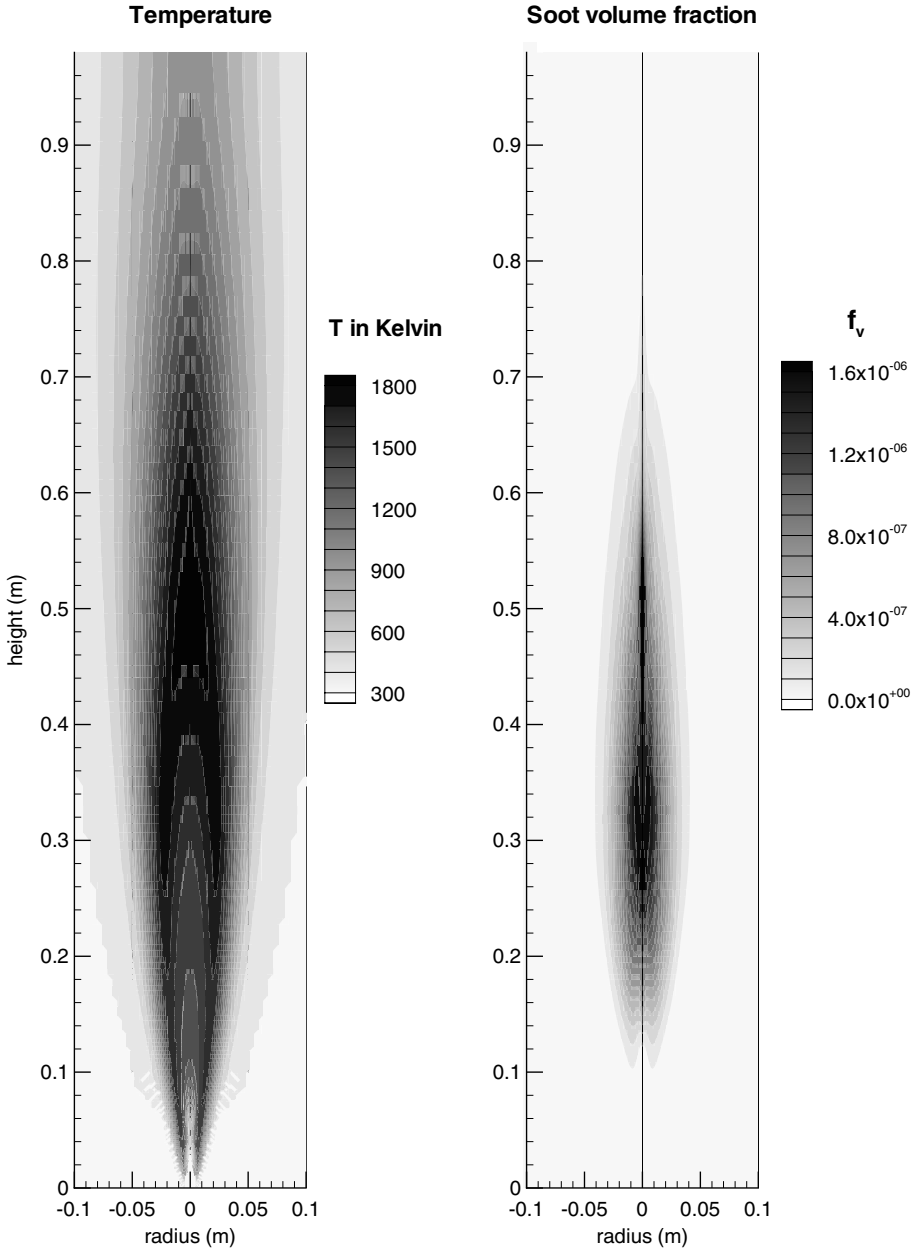

Fig. 2. Temperature and soot volume fraction fields in the ethylene–air flame.

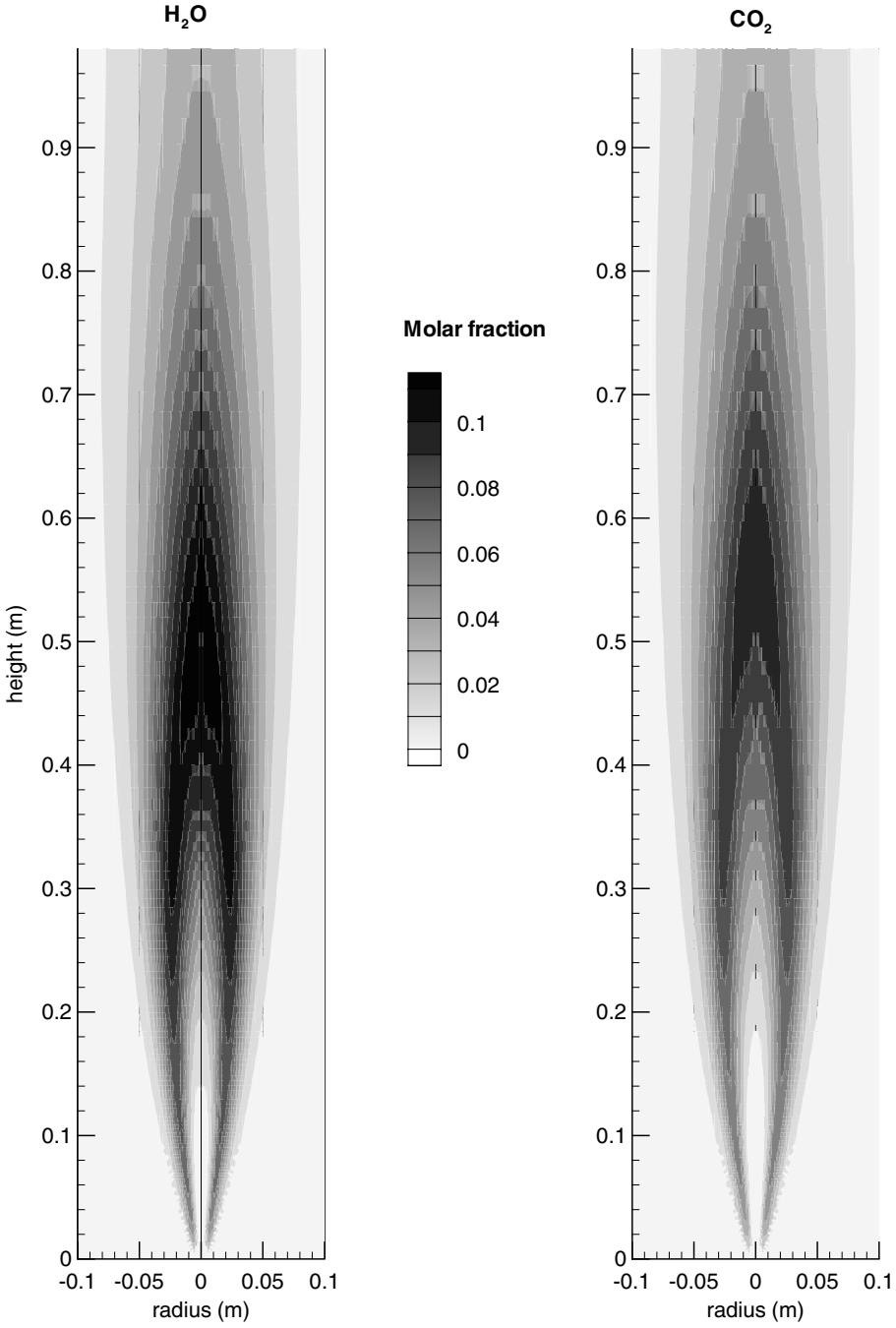

Fig. 3. H_2O and CO_2 molar fraction fields in the ethylene–air flame.

volume fraction field and the H_2O and CO_2 concentration fields. It is worth noting that, due to post-flame oxidation, the highly sooting zone does not extend as far as the burnt gas zone. Fig. 4 gives the profiles of temperature, soot volume fraction and H_2O and CO_2 concentrations, 50 cm above the ethylene inlet section. The peak of soot concentration is located in a very narrow zone at the center of the flow which corresponds to the fuel side of the diffusion flame. The total radiative loss of the initial empirical model, equal to 5760 W, has been obtained by

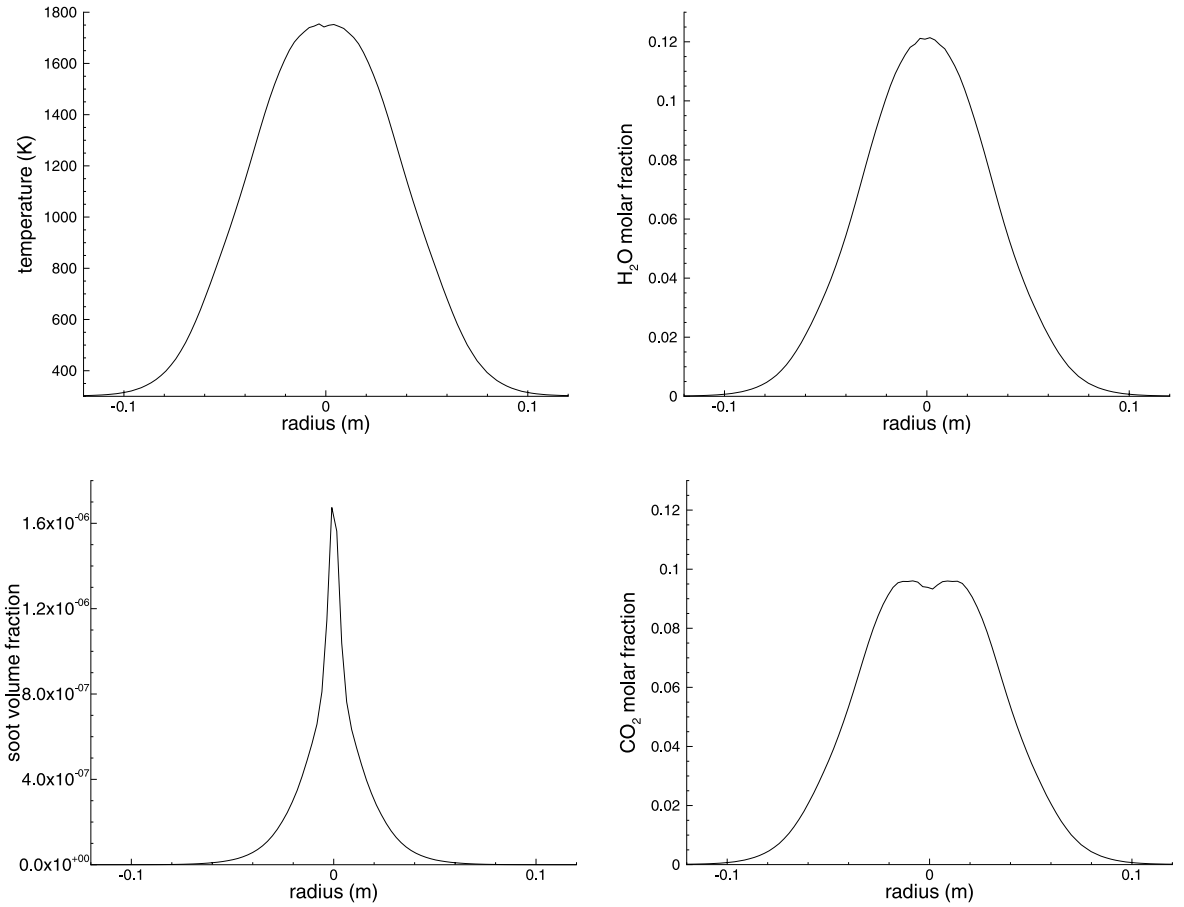

Fig. 4. Profiles of temperature, soot volume fraction, H_2O and CO_2 molar fractions, 50 cm above the burner inlet.

integrating Eq. (18) on the whole flow; it represents 31% of the power introduced by the reaction heat release.

3.3. Joint PDF dimension reduction

The storage of the multidimensional PDF is a real problem. For example, if each direction of the phase space is discretized in 20 intervals, the number of values to be stored is $20^4 \times 150 \times 60$ (the exponent 4 stands for the dimension of the PDF of which the arguments are the temperature, the CO_2 concentration, the H_2O concentration and the soot volume fraction and the two last numbers are the mesh numbers). That makes a storage of 11.5 Gb. In order to decrease it, some assumptions were made so that a PDF of lower dimension could be used.

As the major burnt products are created by very sudden reactions the PDF dimension can be reduced. Concerning the major species, it is assumed that, in terms of progress variable ξ, there is at a given point and at a given time either fresh gas ($\xi = 0$) or burnt gas at equilibrium ($\xi = 1$). Under this assumption, the thermochemical parameters associated with the major species depend only on ξ and on the mixture ratio r. Moreover, when ξ is zero, the medium is cold and contains neither soot particles nor absorbing gases. If we neglect the ethylene absorption, the medium is then non-participating. The optical properties associated with the major species have thus to be determined only when ξ is equal to 1. The ethylene absorption could be taken into account but we neglect it because, in our case, the volume filled with unburned ethylene is very small.

The above assumption is valid for the temperature. It can be seen in Fig. 5 that, for three different fluid packets, which are typical of the packets made up of burnt products, the temperature is a function of the mixture ratio but is relatively independent of the pocket itself. The previous assumption also applies to the CO_2 and H_2O concentrations. On the other hand, Fig. 5 shows that this assumption does not apply to the soot volume fraction f_V. Consequently, the considered PDF only depends on the three parameters ξ, r and f_V. In

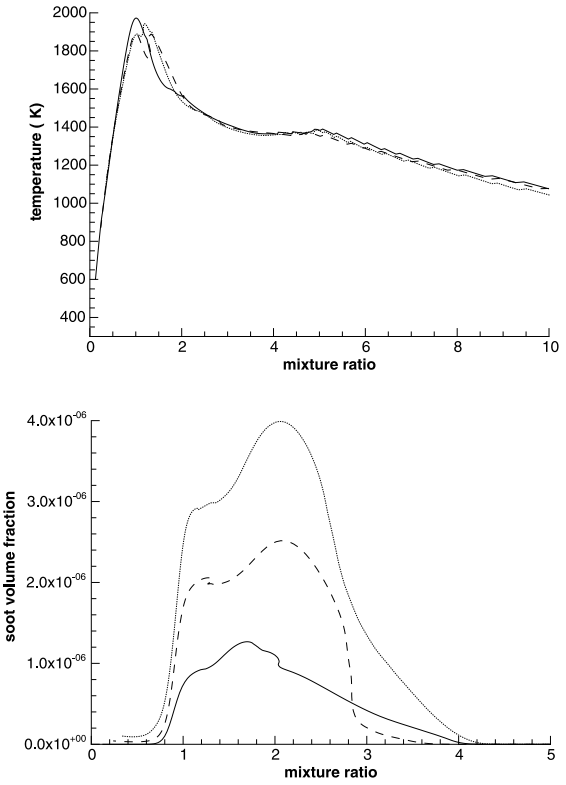

Fig. 5. Temperature (top) and soot volume fraction (bottom) versus mixture ratio in three typical particles made up of burnt gas (the mixture ratio is equal to 1 at stoichiometry).

practice, the PDF has to be stored only when ξ is equal to 1, because the medium is transparent when ξ is equal to 0. Comparisons are carried out in Section 4.2 between calculations with and without TRI. In order that small errors introduced by the PDF reduction do not bias these comparisons, the averaged fields of temperature and H_2O and CO_2 concentrations, used for the calculations without TRI, have been directly calculated from the reduced PDF. In these conditions, all the averaged fields are coherent with the PDF used for the TRI calculations. In fact, the initial PDF and the reduced PDF give rigorously the same field of soot volume fraction.

3.4. Radiative characterization of the flame

For gas radiation, only H_2O and CO_2 are taken into account. Gas radiative properties are treated in a correlated manner by a CK model [25–28] based on the parameters of Soufiani and Taine [22]. These parameters have been generated for applications at atmospheric pressure in the temperature range 300–2500 K. For H_2O, 44 joined spectral bands, with variable width, are considered between 150 and 9200 cm^{-1}. However, CO_2 absorbs radiation in only 17 of these bands. The use of a 7-points Gauss quadrature for each gaseous component leads to 1022 pseudo-spectral points, since 49 quadrature points are used in the 17 overlapping bands. It is worth noting that the Monte Carlo approach allows us to use this accurate spectral model without increase of the computational time compared to a much more simple one.

For the radiation of the soot particles, 71 spectral bands have been introduced between 150 and 20,000 cm^{-1}, of which 44 are common to the gas. The scattering by the soot particles is neglected because of the small value of the size parameter $x = 2\pi R/\lambda$ associated with the primary soot particles. R is the radius of these primary soot particles and λ is the order of magnitude of the wave length radiation. In absence of agglomeration phenomena, the parameter x lies typically in the range (0.06–0.18). If required, the treatment of the scattering phenomena would not significantly increase the computational time, assuming that the scattering parameters associated with soot agglomerates are well known. The chosen spectral soot absorption coefficient (in m^{-1}) is given by

$$\kappa_v^{\text{soot}} = 550 v f_V, \tag{19}$$

where v is the wavenumber (in cm^{-1}) and f_V the soot volume fraction, as discussed in Ref. [23].

In the radiative calculations, all the boundaries of the calculation domain, except the two vertical planes, borders of the 5° sector, on which periodicity conditions are set, are open boundaries. We assume that no radiative energy enters from outside through these open boundaries. This is a simplifying assumption for the upper horizontal boundary, based on the fact that the temperature and the soot concentration decrease rapidly beyond this boundary, due to the mixing with air.

4. Results

As mentioned in Ref. [20], one single Monte Carlo calculation allows us to obtain the results corresponding to different approaches, i.e. the forward method (FM), the emission reciprocity method (ERM) and the absorption reciprocity method (ARM). The FM is the usual Monte Carlo method where the energy balance in a cell is made from all optical paths crossing this cell, along which only one propagation direction is considered. On the other hand, the ERM and ARM are based on the reciprocity principle, which means that the energy propagation is considered in both opposite directions along a given optical path. In the ERM, the optical paths are issued from the cells where the energy balances are made while, in the ARM, the optical paths are issued from the other cells. In the case of our diffusion flame and of the chosen boundary conditions, the use of the ARM is impossible because the volume cells can not emit according

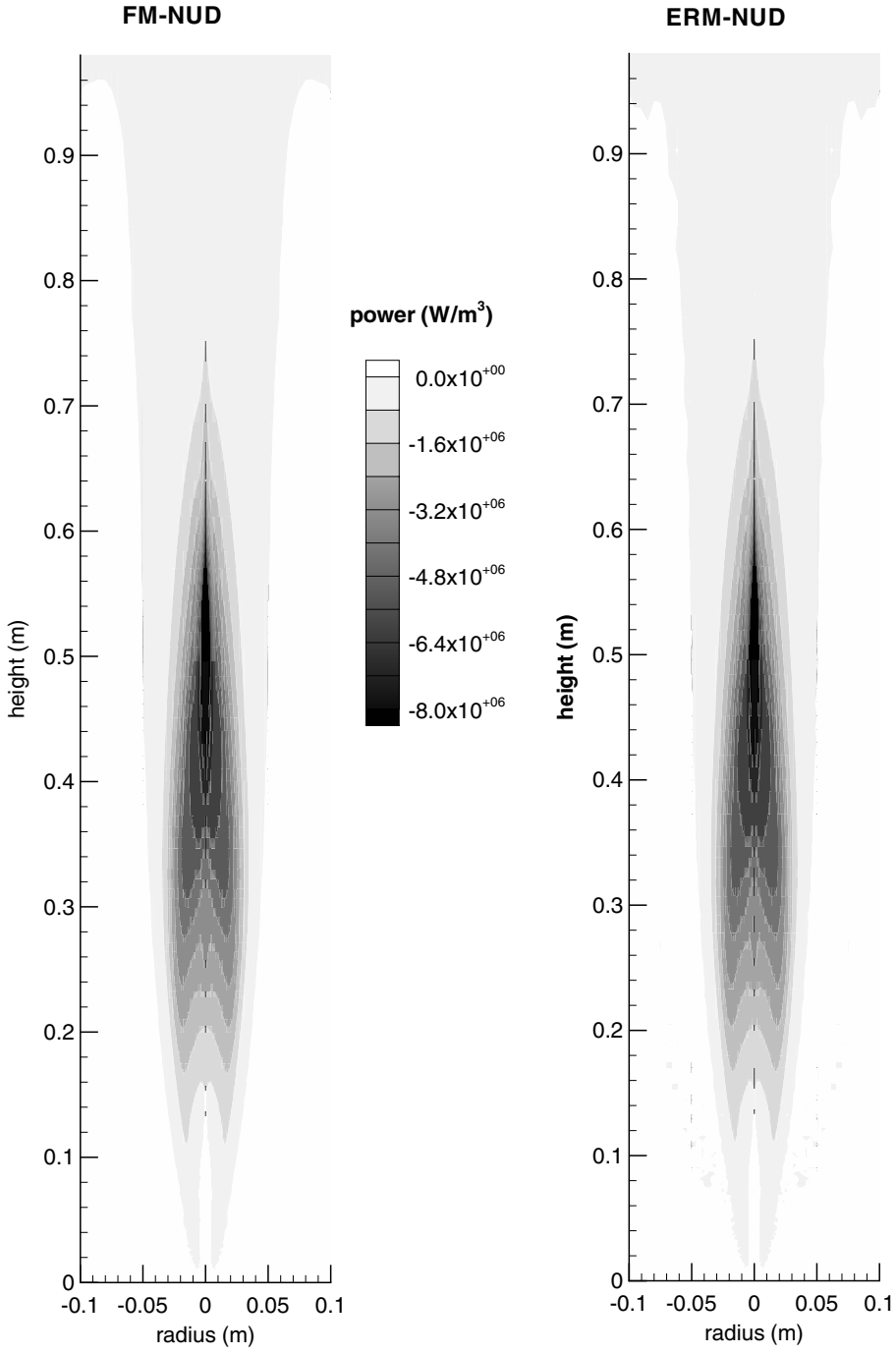

Fig. 6. Radiative power field in the diffusion flame obtained with the numerical techniques FM-NUD and ERM-NUD (calculations based on the averaged field).

to the reciprocity principle the power which is transmitted through an open boundary. Therefore only the results of the FM and ERM will be compared.

The number of optical paths emitted by each cell has been chosen proportional to the radiative energy emitted by this cell (without taking into account the energy

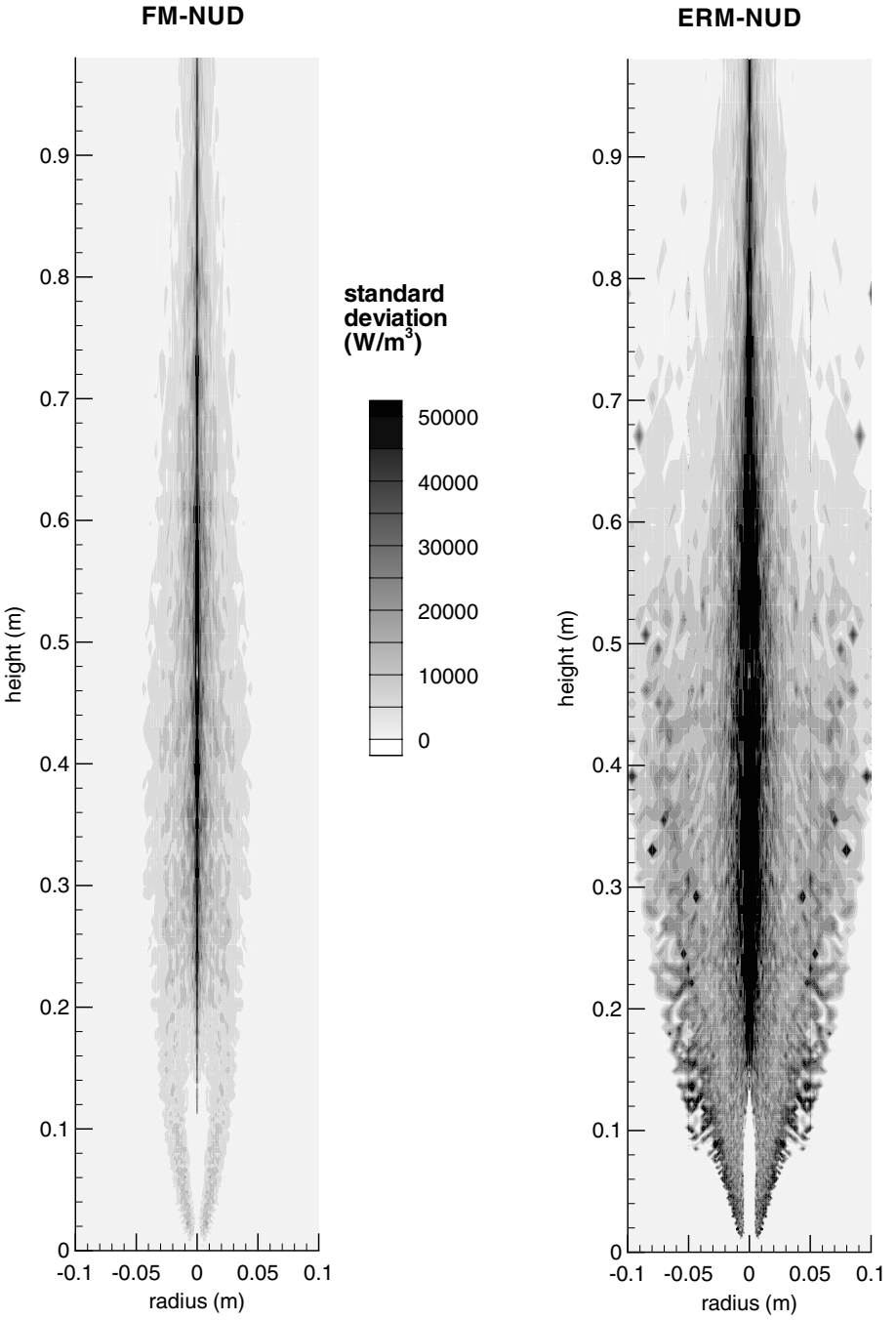

Fig. 7. Standard deviation on the radiative power in the diffusion flame for the numerical techniques FM-NUD and ERM-NUD (calculations based on the averaged field).

self-absorbed in the cell). This technique of emission treatment, called non-uniform distribution (NUD), has been preferred to the uniform distribution (UD) technique because the considered diffusion flame is similar to the case 6 of the benchmark of Ref. [20] for which the NUD is the best choice.

4.1. Results based on the averaged field

We consider here radiative transfer calculations in the flame defined in Section 3.1. In a first step, The calculations have been carried out without taking into account the TRI. 10^7 optical paths, statistically independent, have been

generated. They have been gathered in 10 sets of 10^6 tracked optical paths in order to obtain 10 independent calculations of the radiative power field. A rough estimation of the radiative power standard deviation is then deduced from these 10 results. For a given number of optical paths, a larger number of independent calculations would give less noise in the estimation of the standard deviation but a higher value of it since these calculations would be less accurate. We have checked that the standard deviation roughly decreases as the inverse of the square root of the number of tracked optical paths. Fig. 6 gives the radiative power fields obtained by the FM and ERM which are practically identical. The radiative power integrated on the whole calculation domain, a 5° sector, is equal to −58.7 W (−4230 W for the whole flame) regardless of the method. It is worth noting that the ERM does not give the radiative flux on the open boundaries, which do not emit. With the FM, the outwards radiative flux is strictly equal to the absolute value of integrated radiative power, that is 58.7 W. Fig. 7 gives the standard deviation maps for the FM and ERM. The standard deviation of the FM results is clearly less. This is in agreement with the conclusion of Ref. [20] where the NUD-FM has been found the most accurate approach for the case 6 of the benchmark. The standard deviation is maximum on the axis because the volumes of the cells are there small and the numbers of optical paths involved in the statistics of these cells are consequently low. These facts are confirmed in Fig. 8 which gives the profiles of the radiative power and of its standard deviation, 50 cm above the ethylene inlet section. It is worth noting that a good estimation of the standard deviation associated with 10^7 optical paths can be obtained by dividing by a factor $10^{1/2}$ the results of Figs. 6 and 7.

4.2. Results based on the turbulence–radiation interaction

The same approach as in Section 4.1 has been carried out by taking into account the TRI with 10 independent sets of 10^6 tracked optical paths. Only the results of the most efficient numerical technique, the FM-NUD, have been analyzed. Fig. 9 shows the emitted power fields with TRI and without TRI, $\langle P_q^e \rangle$ and P_q^e defined respectively by Eq. (9) and an equation similar to Eq. (16) with $\langle T_q \rangle$ and $\langle c_q \rangle$ in place of $T_{i_{p1}}$ and $c_{i_{p1}}$. In the center of the flame, the emission is larger without the TRI but the emitting zone is wider with the TRI. Indeed, the emission is significant when the temperature and the soot concentration are simultaneously high. Near the flame front, on the fuel side, these conditions can be found for the averaged values and therefore the emission without TRI is large. With the TRI, an averaged state where the mean temperature and soot concentration are simultaneously high corresponds to a set of instantaneous states where the mixture ratio is alternately much higher than one or slightly lower than one. In the first case, the soot concentration is high but the temperature is low; in the second case, the temperature is high but the soot concentration is low. In both cases, these conditions are not very favorable for emission. Consequently, the emission is lower with the TRI in the center of the flame. On the other hand, on the air side, the average temperature decreases when the distance to the axis increases and, without TRI, the emission decreases rapidly. With the TRI, a state of relatively low average temperature can be characterized by successive instantaneous states of very low temperature and relatively high temperature. Due to the non-linearity of the emission law, these conditions are favorable to the radiative emission. Consequently, the emission zone is wider with the TRI than without it. This is confirmed in Fig. 10, which gives the profiles of the emitted and of the radiative powers with and without the TRI, 50 cm above the ethylene inlet section. It is worth noting that, because the peaks of emitted power are located on the axis and because the geometry is axisymmetric, the intensities of these peaks influence less the global power emitted by the flame than the widths of

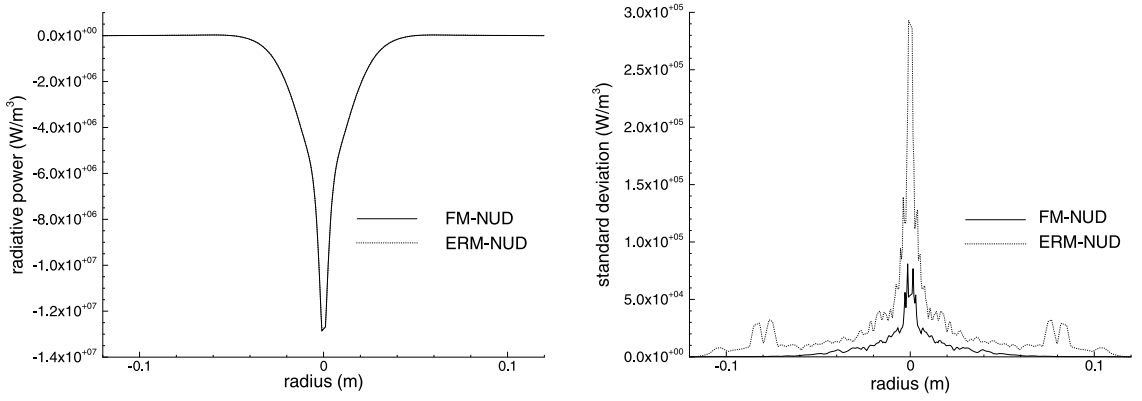

Fig. 8. Profiles of the radiative power and of its standard deviation, 50 cm above the ethylene inlet (calculations based on the averaged field).

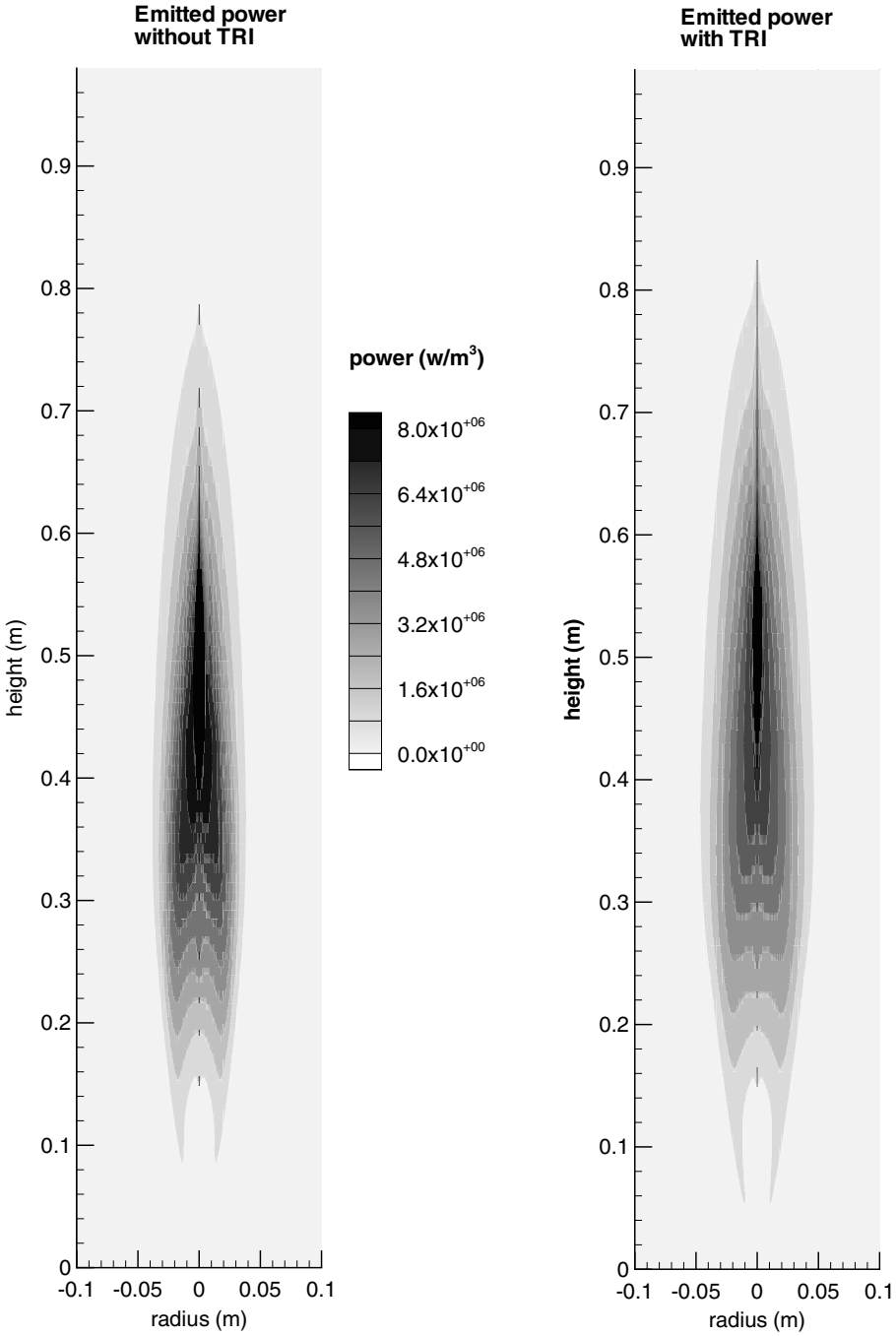

Fig. 9. Emitted power field in the diffusion flame without TRI (on the left) and with TRI (on the right).

the emitting zones. This remark is also valid for the radiative power field shown in Fig. 11. Therefore, the global emitted power is higher with the TRI (123.5 W for a 5° sector and 8890 W for the flame) than without the TRI (respectively, 93.0 and 6700 W). The corresponding radiative powers are −76.7 and −5550 W with the TRI and only −58.7 and −4230 W without the TRI.

The global results are summarized in Table 1. It is worth noting that the radiative loss is an important fraction of the reaction heat release: with the TRI, the

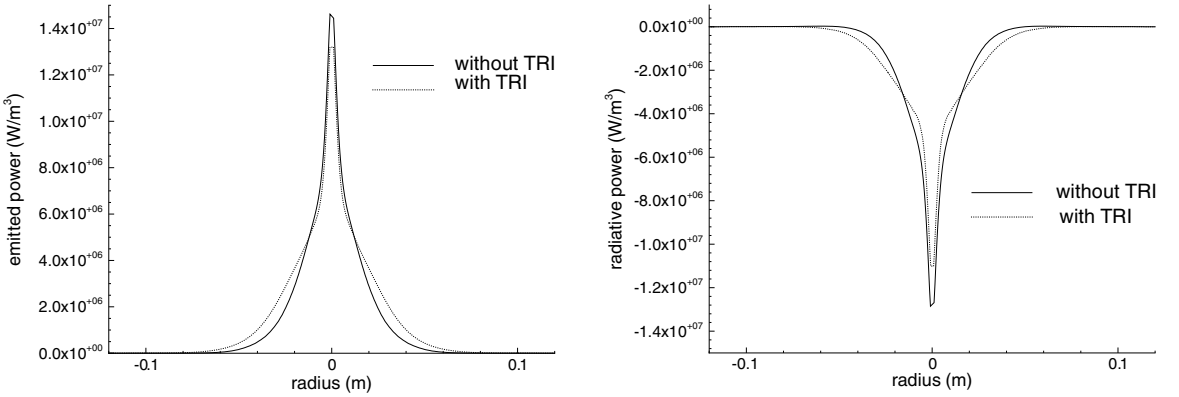

Fig. 10. Profiles of the emitted power and of the radiative power, 50 cm above the ethylene inlet.

total radiative loss is 5550 W, i.e. 30% of the reaction heat release. The power absorbed in the flame by the soot particles and by the burnt gas, H_2O and CO_2, is also important compared to the emitted power. Consequently, the assumption of optically thin medium is not valid in our case. Moreover, the radiative power is 31% higher with the TRI than without it. As expected, because of the non-linearity of the radiative emission law, the turbulence strongly increases the global radiative transfer in the flame. This can be clearly seen in Fig. 12, which gives the radiative flux on the open vertical boundary. The flux calculated with the TRI is higher at any position above the burner. The standard deviation of this flux is also much higher with the TRI. In fact, the number of parameters involved in the modeling with the TRI is larger and thus the accuracy of the Monte Carlo method is lower than without the TRI, though acceptable. The noise of the standard deviation lines is due to the low number (equal to 10) of independent calculations used to evaluate this quantity.

Calculations with the TRI but using an uncorrelation assumption (UA) have also been carried out for comparison. According to this assumption, the absorption properties in the turbulent structure containing the emission point are calculated independently of the emission properties. Moreover, the absorption coefficient of each cell is obtained in a deterministic manner by averaging over all the possible values of ξ, r and f_V, by using the previously defined PDF. This uncorrelation assumption leads to an underestimation of the absorption and hence to a moderate error on the radiative power (9%), as shown in Table 1.

For TRI calculations, the sensitivity of the results to the turbulent integral length has been estimated. For that purpose, two calculations have been carried out by dividing and multiplying respectively the integral length l_t initially deduced from the k–ϵ model by a factor 3. For large, standard and small l_t, the global radiative powers are 67.6 W (4867.2 W for the whole flame), 76.7 W (5522.4 W for the whole flame) and 81.1 W (5839.2 W for the whole flame) respectively. This shows that the radiative transfer is very sensitive to the turbulence field, especially to the value of l_t. Of course, the difference between these results arises only from the absorbed power. It is worth noting that, for small values of l_t, the coherent turbulent structures tends to become optically thin. When this limit is reached, the results are close to those obtained with the UA, if the meshes of the calculation grid are also optically thin. In this case, the OTFA could be used as well.

4.3. Influences of soot particles and gaseous species

The influence of the soot particles and of the gaseous species on the radiative transfer has been studied. Some partial calculations of the radiative transfer in the flame taking into account, respectively, the soot particles only, the gaseous species only, H_2O only and CO_2 only have been carried out and compared. The results are summarized in Table 2. The global emission of the gas, dominated by CO_2, is of the same order of magnitude as the soot emission. It is worth noting that the burnt gas, CO_2 and H_2O, are distributed everywhere in the flame while the soot particles are located in a small volume, on the fuel side where the conditions of temperature and mixture ratio are both favorable to their formation. At the location of the soot particles, the soot emission is much higher than the gas emission. At other locations, only the gaseous species practically emit radiation. It appears also that the part of the emitted energy which is absorbed in the flame is not negligible for all the components and is even very large in the case of CO_2. This result invalidates again the assumption of optically thin medium in this flame. Because the self-absorption phenomenon is higher in gas than in soot, the global radiative loss of the flame due to the soot particles appears to be larger than the global radiative loss due to the gas. However, gas radiation plays a prominent role

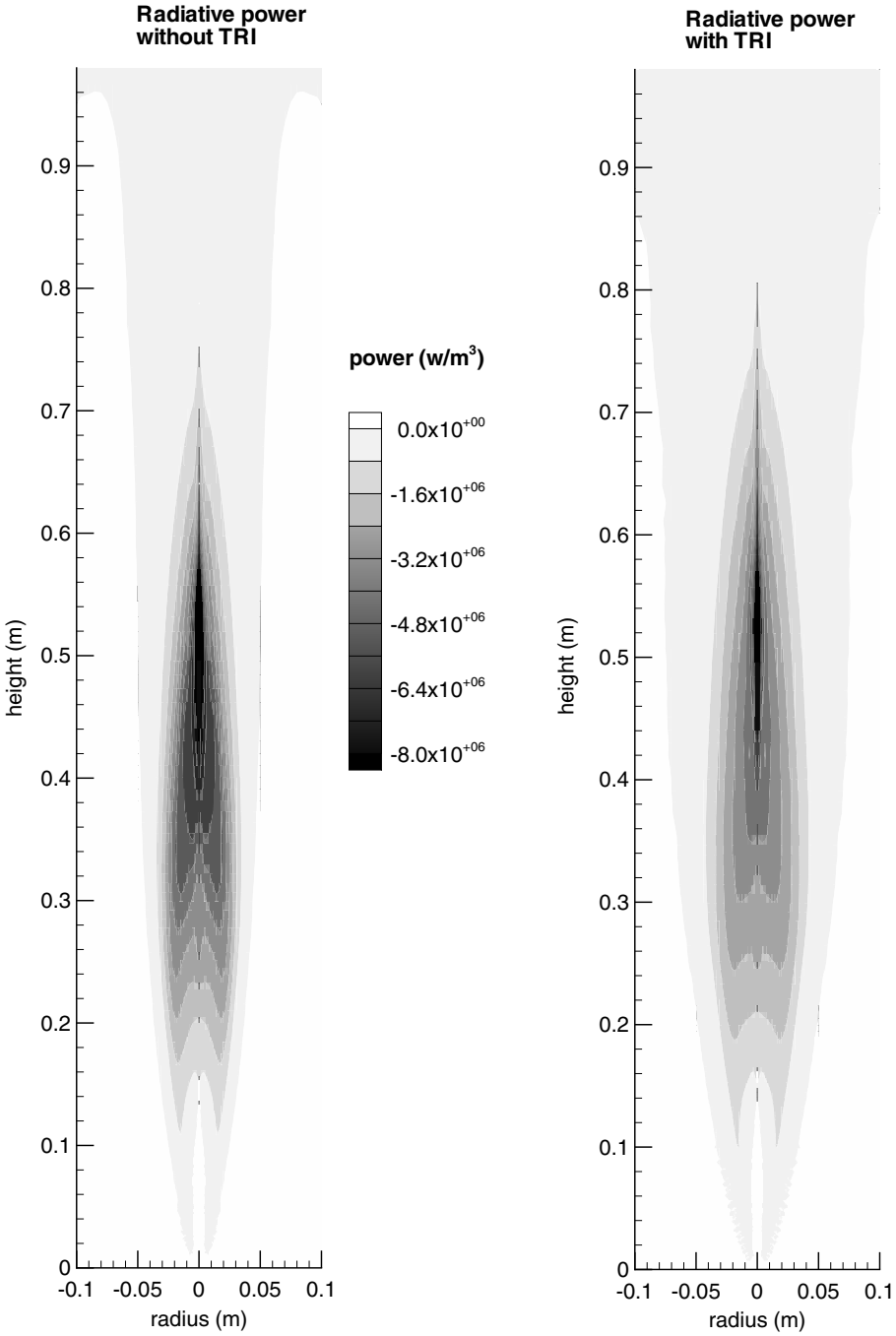

Fig. 11. Radiative power field in the diffusion flame without TRI (on the left) and with TRI (on the right).

in the energy balances inside the flame, except in the soot location region.

The computation time for a radiative transfer calculation involving 10^7 optical paths is about 10^4 s on one processor of a NEC SX5, regardless of the physical model. It does not depend strongly on the physical model because the generation of random numbers requires much less computation time than the geometrical treatment of the optical paths, which is common to all the models. It is worth noting that this treatment could be easily optimized. In comparison, the computation time of both RANS and Lagrangian calculations is

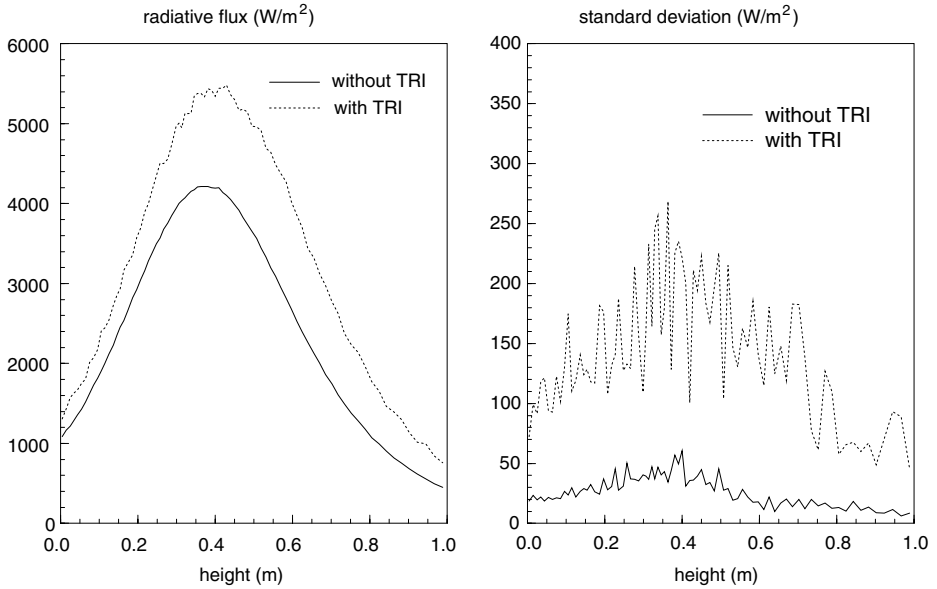

Fig. 12. Radiative flux on the vertical open boundary.

Table 1
Influence of the turbulence–radiation interaction (TRI), of the uncorrelation assumption (UA) and of the turbulent integral length on the global radiative power

	Emitted power (W)	Absorbed power (W)	Radiative power (W)
Without TRI	93.0	34.3	−58.7
TRI and UA	123.5	39.9	−83.6
With TRI	123.5	46.8	−76.7
TRI with l_t divided by 3	123.5	42.4	−81.1
TRI with l_t multiplied by 3	123.5	55.9	−67.6

Table 2
Influence of the components of the semi-transparent medium on the global radiative power

	Soot and gas		Only soot		Only gas		Only H_2O		Only CO_2	
	No TRI	TRI	No TRI	TRI	No TRI	TRI	No TRI	TRI	No TRI	TRI
Emitted power (W)	93.0	123.5	43.7	59.3	49.3	64.2	9.7	12.8	39.6	51.5
Absorbed power (W)	34.3	46.8	3.4	8.8	29.8	35.8	2.3	2.5	27.3	33.1
Radiative power (W)	−58.7	−76.7	−40.3	−50.5	−19.5	−28.4	−7.4	−10.3	−12.3	−18.4

about 7×10^4 s and the complete calculation coupling CFD, chemistry and radiative transfer is expected to require less than five iterations.

5. Conclusion

The radiative transfer in the considered open ethylene diffusion flame is very significant. Due to the non-linearity of the radiation emission, the turbulence strongly increases this radiative transfer so that the turbulence–radiation interaction must be taken into account. The simplifying assumption of optically thin medium is not valid for this type of flame. The contributions of the soot particles and of the gas, H_2O and CO_2, to the radiative emission have the same order of magnitude. However, self-absorption by the soot particles, enclosed in a small region, is lower than self-absorption by the gases. Consequently, the soot particles influence more the global radiative loss than the gaseous species.

The Monte Carlo method is very convenient for these radiative calculations, because it allows us to easily treat the turbulence–radiation interaction, as well as to include sophisticated models of gas properties, without computation time increase. Among the different Monte

Carlo approaches, the forward-method associated with a non uniform distribution of the source points of the tracked optical paths is the most efficient approach for our configuration, because the optical thickness of the flame is moderate.

One key point to achieve these calculations is to know the PDF of the quantities involved in the radiative transfer. This joint PDF is bi-dimensional for a given value of the reaction progress variable (0 or 1). The Eulerian–Lagrangian combustion models are an excellent way to get this information.

References

[1] A. de Lataillade, Modélisation détaillée des transferts radiatifs et couplage avec la cinétique chimique dans des systèmes en combustion, Thèse de doctorat, Université Paul Sabatier, Toulouse, France, 2001.

[2] Z. Zhang, O.A. Ezekoye, Soot production rate calculations at elevated pressure in a methane–air jet diffusion flame, Combust. Sci. Technol. 137 (1998) 323–346.

[3] N.W. Bressloff, J.B. Moss, P.A. Rubini, CFD prediction of coupled radiation heat transfer and soot production in turbulent flames, in: Twenty-sixth Symposium (International) on Combustion, The Combustion Institute, 1996, pp. 2379–2386.

[4] C.R. Kaplan, S.W. Baek, E.S. Oran, J.L. Ellzey, Dynamics of a strongly radiating unsteady ethylene jet diffusion flame, Combust. Flame 96 (1994) 1–21.

[5] Y.R. Sivathanu, J.P. Gore, Coupled radiation and soot kinetics calculations in laminar acetylene/air diffusion flames, Combust. Flame 97 (1994) 161–172.

[6] J.H. Kent, D.R. Honnery, A soot formation rate map for a laminar ethylene diffusion flame, Combust. Flame 79 (1990) 287–298.

[7] R. Said, A. Garo, R. Borghi, Soot formation modeling for turbulent flames, Combust. Flame 108 (1997) 71–86.

[8] S.-M. Jeng, M.-C. Lai, G.M. Faeth, Nonluminous radiation in turbulent buoyant axisymmetric flames, Combust. Sci. Technol. 40 (1984) 41–53.

[9] J.P. Gore, G.M. Faeth, Structure and spectral radiation properties of turbulent ethylene/air diffusion flames, in: Twenty-first Symposium (International) on Combustion, The Combustion Institute, 1986, pp. 1521–1531.

[10] J.P. Gore, S.-M. Jeng, G.M. Faeth, Spectral and total radiation properties of turbulent carbon monoxide/air diffusion flames, AIAA J. 25 (1987) 339–345.

[11] J.P. Gore, G.M. Faeth, Structure and radiation properties of luminous turbulent acetylene/air diffusion flames, J. Heat Transfer 110 (1988) 173–181.

[12] M.E. Kounalakis, J.P. Gore, G.M. Faeth, Turbulence/radiation interactions in nonpremixed hydrogen/air flames, in: Twenty-second Symposium (International) on Combustion, The Combustion Institute, 1988, pp. 1281–1290.

[13] K.J. Syed, C.D. Stewart, J.B. Moss, Modelling soot formation and thermal radiation in buoyant turbulent diffusion flames, in: Twenty-third Symposium (International) on Combustion, The Combustion Institute, 1990, pp. 1533–1541.

[14] S. Mazumder, M.F. Modest, A probability density function approach to modeling turbulence–radiation interactions in nonluminous flames, Int. J. Heat Mass Transfer 42 (1999) 971–991.

[15] V.P. Kabashnikov, G.I. Myasnikova, Thermal radiation in turbulent flows—Temperature and concentration fluctuations, Heat Transfer—Sov. Res. 17 (1985) 116–125.

[16] V.P. Kabashnikov, Thermal radiation of turbulent flows in the case of large fluctuations of the absorption coefficient and the Planck function, J. Eng. Phys. 49 (1985) 778–784.

[17] B.R. Adams, P.J. Smith, Modeling effects of soot and turbulence–radiation coupling on radiative transfer in turbulent gaseous combustion, Combust. Sci. Technol. 109 (1995) 121–140.

[18] J.W. Hartick, M. Tacke, G. Friichtel, E.P. Hassel, J. Janicka, Interaction of turbulence and radiation in confined diffusion flames, in: Twenty-sixth Symposium (International) on Combustion, The Combustion Institute, 1996, pp. 75–82.

[19] K.J. Young, J.B. Moss, Modeling sooting turbulent jet flames using an extended flamelet technique, Combust. Sci. Technol. 105 (1995) 33–53.

[20] L. Tessé, F. Dupoirieux, B. Zamuner, J. Taine, Radiative transfer in real gases using reciprocal and forward Monte Carlo methods and a correlated-k approach, Int. J. Heat Mass Transfer 45 (2002) 2797–2814.

[21] B. Zamuner, F. Dupoirieux, Numerical simulation of soot formation in a turbulent flame with a Monte Carlo PDF approach and detailed chemistry, Combust. Sci. Technol. 158 (2000) 407–438.

[22] A. Soufiani, J. Taine, High temperature gas radiative property parameters of statistical narrow-band model for H_2O, CO_2 and CO, and correlated-K model for H_2O and CO_2, Int. J. Heat Mass Transfer 40 (1997) 987–991.

[23] L. Tessé, Modélisation des transferts radiatifs dans les flammes turbulentes par une méthode de Monte Carlo, Thése de doctorat, École Centrale Paris, 2001.

[24] A. Coppalle, D. Joyeux, Temperature and soot volume fraction in turbulent diffusion flames: measurements of mean and fluctuating values, Combust. Flame 96 (1994) 275–285.

[25] R. Goody, R. West, L. Chen, D. Crisp, The correlated-k method for radiation calculations in nonhomogeneous atmospheres, J. Quant. Spectrosc. Radiat. Transfer 42 (1989) 539–550.

[26] A.A. Lacis, V. Oinas, A description of the correlated k distribution method for modeling nongray gaseous absorption, thermal emission, and multiple scattering in vertically inhomogeneous atmospheres, J. Geophys. Res. 96 (1991) 9027–9063.

[27] P. Rivière, A. Soufiani, J. Taine, Correlated-k and fictitious gas methods for H_2O near 2.7 μm, J. Quant. Spectrosc. Radiat. Transfer 48 (1992) 187–203.

[28] P. Rivière, A. Soufiani, J. Taine, Correlated-k fictitious gas model for H_2O infrared radiation in the Voigt regime, J. Quant. Spectrosc. Radiat. Transfer 53 (1995) 335–346.